Proceedings of the 1st international Symposium on AI and Fluid Mechanics
Paper No S11 P12

Data-driven and physics-constrained reduced-order model of the global climate

[1,2]V. Kitsios*; [3]L. Cordier; [4]T. J. O'Kane;

[1] *CSIRO Environment, 107-121 Station Street, Aspendale, Victoria 3195, Australia*

[2] *Laboratory For Turbulence Research in Aerospace and Combustion, Department of Mechanical and Aerospace Engineering, Monash University, Clayton, Australia*

[3] *Département Fluides Thermique et Combustion, CNRS, Université de Poitiers, ENSMA, Institut Pprime, 86360 Futuroscope-Chasseneuil, France*

[4] *CSIRO Environment, Castray Esplanade, Battery Point, TAS 7004, Australia*

Abstract

Whilst weather prediction is a *BigData* problem with many relevant samples over the observed historical period, climate projection is a *SmallData* problem with relatively few samples. Standard machine learning methods, making minimal physical assumptions, have demonstrated recent success in weather forecasting. Typically, functional forms are adopted that capture many types of nonlinearity with many parameters, hence requiring many samples. However, in climate applications there are few relevant samples due to slow time scales, and boundary conditions with trends associated with increasing greenhouse gas emissions. Here we instead make maximal physical assumptions by only allowing the nonlinearity supported by the physics, hence requiring fewer parameters. We develop a reduced-order model (ROM) of the global atmosphere by projecting the equations of motion onto a set of proper orthogonal decomposition (POD) modes. This transforms a system of partial differential equations dependent upon time and space, into a system of ordinary differential equations dependent upon time and POD mode index. The POD modes are calculated for the atmospheric velocity and temperature fields sourced from the Climate Analysis Forecast Ensemble data assimilation system. This data comprises of 96 three-dimensional model realisations of the Earth from 1960 to 2020, which have been corrected on the basis of real-world observations. The ROM coefficients are calculated via an optimisation procedure that minimises the forecast error of each POD mode. Our ROM reproduces the large-scale atmospheric variability at a fraction of the computational cost.

Keywords: Climate; Atmosphere; Reduced-Order Model; Galerkin Projection; Optimisation

Introduction

To navigate a transition to a lower carbon economy stakeholders require assessments of the physical climate risk for many future economic and hence carbon emissions scenarios. General circulation models (GCMs) undertake the simulations of the climate that provide the necessary data to make such assessments. However, due to their computational cost, it is only practical to simulate a small subset of the possible future outcomes.

One solution is to develop data-driven, rapid and cheap reduced order models (ROMs) of the climate. Here we do so for the global atmosphere. Possible approaches range from black-box methods [1], to the more physically constrained ones adopted here. We perform a Galerkin projection, where the partial differential equations (PDEs) governing the global atmosphere are projected onto proper orthogonal decomposition (POD) bases. This transforms the PDEs evolving the flow in time and three-dimensions of space, into a set of ordinary differential equations (ODEs) governing the contribution of each POD mode in time. This reduces the computational expense immensely. The model coefficients of the ROM are calculated using a regression approach [2]. This technique was adopted in [3] to develop the first ever POD ROM of the global oceans, which captured seasonal and inter-annual climate variability. This approach was applied to the global atmosphere in [4], which additionally captured mean trends due to the contribution of climate change, but with only a dynamically evolving velocity field.

Here we form a fully coupled POD ROM of the global atmosphere with dynamical fluctuating velocity and temperature fields. The POD ROM is developed using data from the Climate Analysis Forecast Ensemble reanalysis [5], denoted by CAFE-60. In CAFE-60 real-world observations of the Earth system are exploited to continually correct an ensemble of 96 simultaneous GCM simulations. It provides three-dimensional (3D) fields from 1960 to 2020 for each of the 96 ensemble members. In the following section we characterise the trends, seasonality and multi-year variability in CAFE-60. The POD bases are then presented. The derivation of the POD ROM, and

*Corresponding Author, V. Kitsios vassili.kitsios@csiro.au

calculation of the model coefficients, are then outlined. Finally, the POD ROM output is validated against the underlying data.

Flow Field Characterisation

In CAFE-60 the atmosphere, ocean, land, sea-ice and bio-geo-chemical components are all simulated in a coupled manner. For the present POD ROM we only require the fields from the atmosphere. This output is provided on *21* vertical levels. The structured grid has a resolution of 2° in latitudinal direction and 2.5° in longitude. The time step size in the atmospheric component of the GCM was 30 minutes. The output used here, however, is monthly averaged. The boundary conditions have periodic and aperiodic components, which are respectively associated with orbit of the Earth around the Sun, and the growing greenhouse gas concentrations. These forcings result in the observed climate trends, seasonality, and inter-annual variability.

To characterise the flow we first define the state vector $\boldsymbol{q}=(\boldsymbol{u},T)$, comprising of the temperature (T), and horizontal velocity vector $\boldsymbol{u}=(u,v)$, with eastward zonal (u), and northward meridional (v) velocity components. Note, we require only the horizontal velocity components because when using the hydrostatic approximation in the global atmosphere, one does not evolve the vertical velocity, but rather diagnoses it the from the horizontal components. The flow of an individual ensemble member or the ensemble averaged flow can be decomposed according to

$$\boldsymbol{q}(\boldsymbol{x},t) = \bar{\boldsymbol{q}}^{\Delta}(\boldsymbol{x},t) + \tilde{\boldsymbol{q}}(\boldsymbol{x},t) + \boldsymbol{q}'(\boldsymbol{x},t) \quad \#(1)$$

where $\bar{\boldsymbol{q}}^{\Delta}(\boldsymbol{x},t)$ is the trend, and $\tilde{\boldsymbol{q}}(\boldsymbol{x},t)$ is the seasonal part with a 1-year phase period of zero time mean. The $\boldsymbol{q}'(\boldsymbol{x},t)$ term, represents the residual inter-annual fluctuations, which is characterised using POD in the following section. The trend is modelled akin to an approach common in the climate sciences, referred to as pattern scaling [6], according to

$$\bar{\boldsymbol{q}}^{\Delta}(\boldsymbol{x},t) = \bar{\boldsymbol{q}}^{PI}(\boldsymbol{x}) + [T^G(t) - T^G(t^{PI})]\frac{\Delta\bar{\boldsymbol{q}}}{\Delta T^G}(\boldsymbol{x}) \; . \quad \#(2)$$

The pre-industrial state $\bar{\boldsymbol{q}}^{PI}(\boldsymbol{x})$, is averaged over a period from 1963 to $t^{PI} = 1970$. $T^G(t)$ is the centred 10-year rolling mean of the surface averaged temperature. The gradient $\frac{\Delta\bar{\mathbf{q}}}{\Delta T^G}$, quantifies how the 3D state variables change with T^G at each point in space. The average deviations from the trend per month are represented according to

$$\tilde{\boldsymbol{q}}(\boldsymbol{x},t) = \sum_{\vartheta=Jan}^{Dec} \tilde{\boldsymbol{q}}^{\vartheta}(\boldsymbol{x})\, d^{\vartheta}(t) \quad \#(3)$$

where $d^{\vartheta}(t)$ is equal to 1 within month , and zero otherwise. The term $\tilde{\boldsymbol{q}}^{\vartheta}(\boldsymbol{x})$ represents the phase averaged deviation about the trend, for each of the calendar months $\vartheta \in$ *[January,…,December] [Jan,…,Dec] [1,…,12].*

Figure 1 characterises the components in equation (1). The pre-industrial temperature and zonal velocity fields are illustrated in figures 1(d) and figure 1(h), respectively. The black line in figure 1(a) is the monthly globally-averaged surface temperature. It clearly illustrates a growing trend, the seasonality and inter-annual variability. The red line in this plot is a 10-year moving average ($T^G(t)$). Figure 1(b) illustrates the detrended timeseries, where the red line in figure 1(a) is subtracting away from the black one. The anomalies (or fluctuations) about the detrended timeseries are calculated by subtracting away its phase average. The anomalous timeseries is shown in figure 1(c). The mean response of the temperature field with respect to $T^G(t)$ is illustrated in figure 1(e), indicating an increase in temperature globally. Figure 1(i) illustrates the response of the zonal velocity field, and indicates a shift of southern hemisphere eastward jet toward the south pole. The standard deviation of the seasonal cycle is illustrated for the temperature and zonal velocity fields in figures 1(f) and 1(j), respectively. The standard deviation of the associated anomalies are illustrated in figures 1(g) and 1(k). For both variables the standard deviation of the seasonal cycle is significantly larger than that of the anomalies. This indicates that the difference from one season to the next, is larger than the difference from one year to the next for a given season. However, the ability to forecast the anomalous fields is essential in order to make predictions more skilful than simply prescribing the average seasonal state. The anomalous component at each point in space are decomposed into a series of POD modes in the following section, and will be simulated in the POD ROM to follow.

*Corresponding Author, V. Kitsios vassili.kitsios@csiro.au

Proper Orthogonal Decomposition

The computationally efficient snapshot POD method [7] is used to calculate two separate PODs, one for the anomalous 3D two-component velocity field, and another for the anomalous 3D scalar temperature field given by

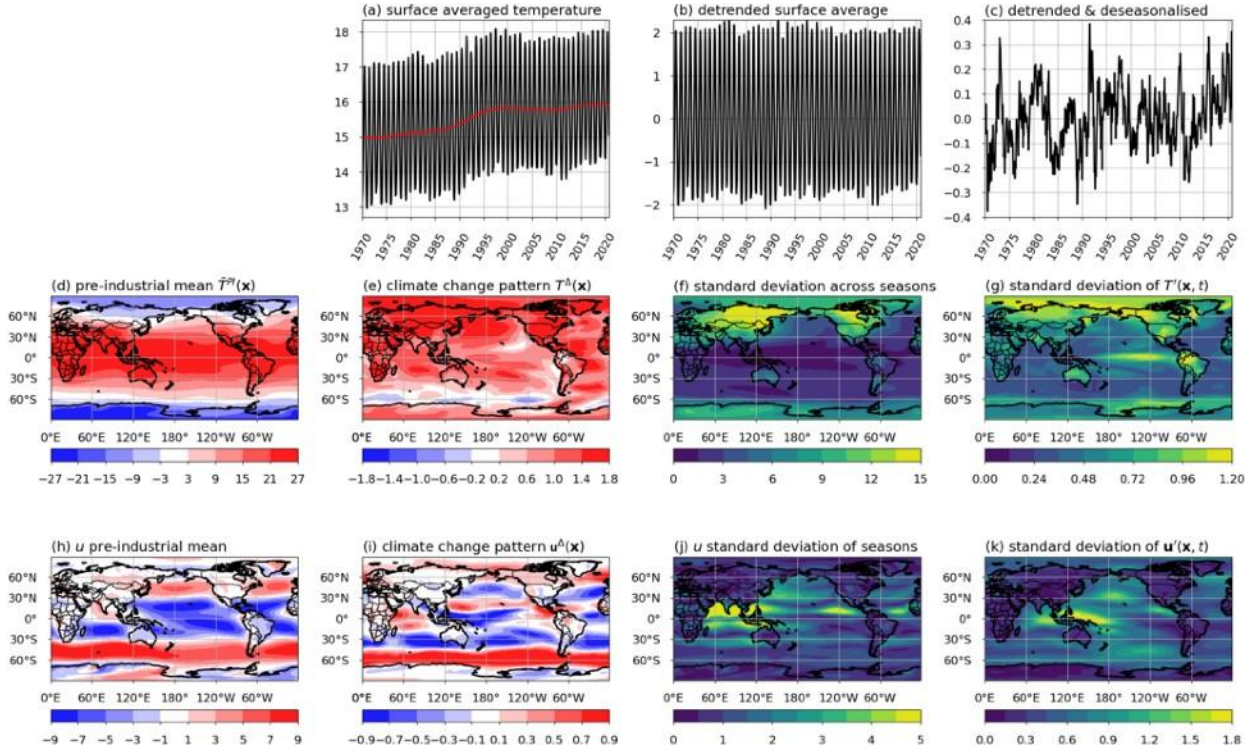

Figure 1 *Characterisation of the CAFE-60 reanalysis at the lowest vertical level. Time series of globally averaged surface temperature: (a) monthly and annual; (b) detrended monthly; (c) detrended and deseasonalised. Surface temperature field: (d) pre-industrial mean; (e) climate change gradient; (f) standard deviation of seasons; and (g) standard deviation of anomalies. Surface zonal velocity field: (h) pre-industrial mean; (i) climate change gradient; (j) standard deviation of seasons; and (k) standard deviation of anomalies.*

$$\boldsymbol{u'}(\boldsymbol{x}, \boldsymbol{t}) = \sum_{n=1}^{Nu} \boldsymbol{\mathcal{U}}^{(n)}(\boldsymbol{x})\ a^{(n)}(t) \#(4)$$

$$T'(\boldsymbol{x}, \boldsymbol{t}) = \sum_{n=1}^{NT} T^{(n)}(\boldsymbol{x})\, b^{(n)}(t) \#(5)$$

where N_U and N_T are the numbers of velocity and temporal POD modes retained in their respective reconstructions. The temporal POD velocity, $a^{(n)}(t)$, and temperature, $b^{(n)}(t)$, modes have units of ms^{-1} and ^{o}C respectively. They have zero mean, and are scaled to represent the variance of each mode. The spatial POD temperature modes, $T^{(n)}(\boldsymbol{x})$, are unitless with orthogonality properties of $\langle T^{(n)}(x), T^{(m)}(x) \rangle_T = \delta_{nm}$, where δ_{nm} is the Kronecker delta function. The angled brackets denote an inner product integrating the product of the spatial modes over the domain volume. Likewise, the spatial POD velocity modes, $\boldsymbol{\mathcal{U}}^{(n)}(\boldsymbol{x}) \equiv (\mathcal{U}^{(n)}(\boldsymbol{x}), V^{(n)}(\boldsymbol{x}))$, are unitless with orthogonality properties of $\langle \boldsymbol{\mathcal{U}}^{(n)}(\boldsymbol{x}), \boldsymbol{\mathcal{U}}^{(m)}(\boldsymbol{x}) \rangle_u = \delta_{nm}$, where this inner product integrates the dot product of these vector quantities.

Figure 2 illustrates the velocity POD basis in the left column and the temperature POD in the right. In the top row, the black line illustrates the percentage of variance per mode, with the shaded green representing the cumulative percentage variance. For both POD spectra, the first 10 modes capture near 70% of the total anomalous variability. The first temporal mode is illustrated in the second row. Recall CAFE-60 contains 96 separate realisations of the Earth every month. The grey shaded region illustrates the range of POD mode contributions across all of the ensemble members, and the solid black line the ensemble averaged contribution. The third row of plots illustrate the

*Corresponding Author, V. Kitsios vassili.kitsios@csiro.au

first spatial modes are at the lowest vertical level. For the velocity decomposition we illustrate the meridional velocity component, noting that there is another pattern for the zonal velocity component. The temperature mode possesses large scale features reminiscent of the El Niño and La Niña cycle in the tropical Pacific. As the mode indices increases, the variability of each mode decreases, dominant temporal frequencies increase, and the dominant spatial features move further away from the equator. The POD modes are the bases upon which the POD ROM are projected.

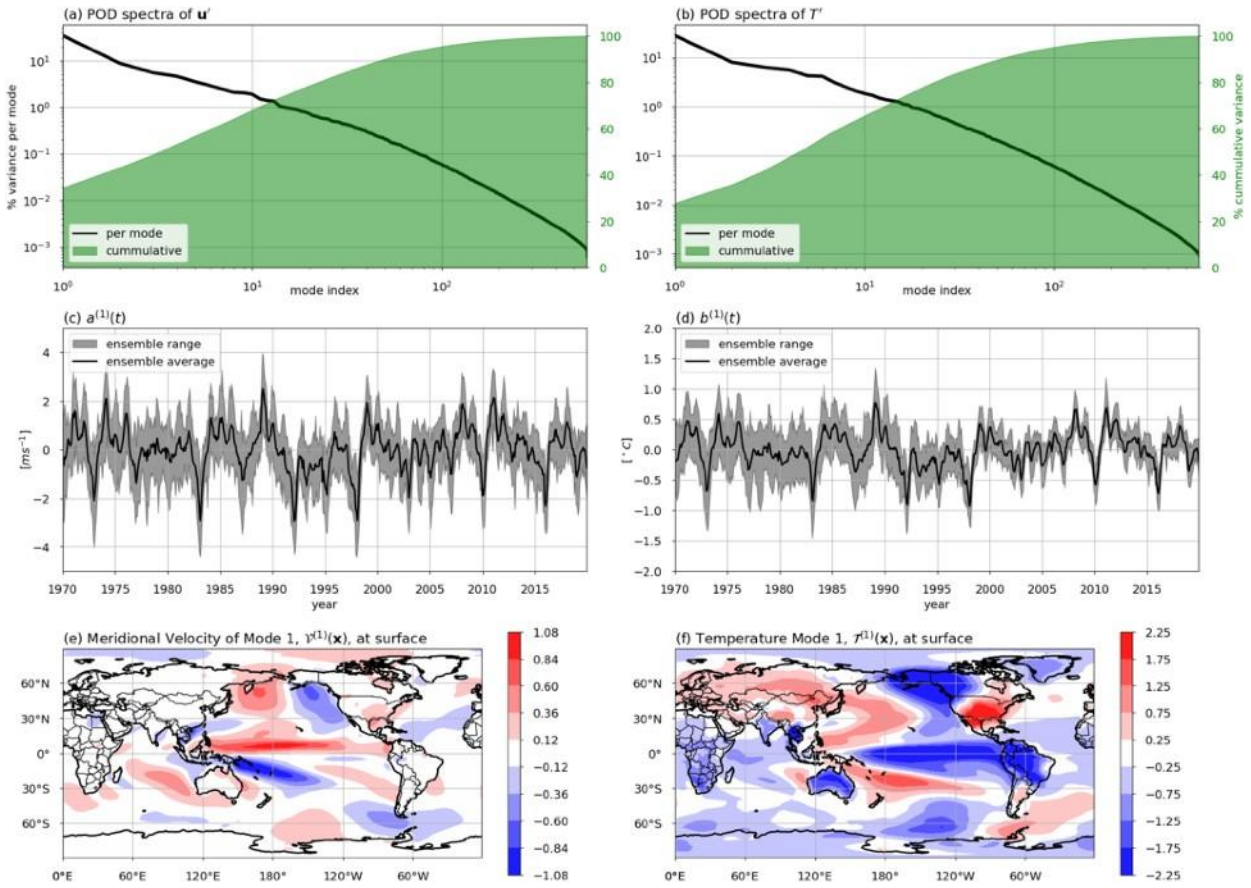

Figure 2 *POD mode bases. Velocity: (a) POD spectra; (c) first temporal mode; and (e) meridional component of the first spatial mode at the surface.. Temperature: (b) POD spectra; (d) first temporal mode; and (f) first spatial mode at the surface.*

Derivation of the Reduced Order Model

The governing equations required for the POD ROM derivation, constitutes the conservation of mass (continuity), equation of state (ideal gas law), conservation of momentum, and conservation of energy. For the large scale atmosphere, one can make the hydrostatic assumption, where the pressure gradient and the buoyancy terms in the vertical momentum equation dominate. The vertical velocity component is hence not prognostic, but rather diagnosed via the continuity equation. Therefore, one only requires a POD of the horizontal velocity components. After some manipulation, one can show that the equations of motion can be written compactly as

$$\frac{D\boldsymbol{u}}{Dt} = \boldsymbol{\mathcal{N}}(\boldsymbol{u},\boldsymbol{u}) + \boldsymbol{\mathcal{L}}(\boldsymbol{u}) + \boldsymbol{\mathcal{S}}(T) \#(8)$$

$$\frac{DT}{Dt} = \mathcal{M}(\boldsymbol{u},T) + J(\boldsymbol{x},t) \#(9)$$

where $\boldsymbol{\mathcal{N}}(\boldsymbol{u},\boldsymbol{u})$ is a nonlinear function of the velocity field, $\boldsymbol{\mathcal{L}}(\boldsymbol{u})$ a linear function of the velocity field, and $\boldsymbol{\mathcal{S}}(T)$ a linear function of the temperature field, each returning vector quantities. $\mathcal{M}(\boldsymbol{u},T)$ is a nonlinear function of the velocity and temperature fields, which returns a scalar quantity. These functions have their own analytical

*Corresponding Author, V. Kitsios vassili.kitsios@csiro.au

expressions, but their specific form is not required moving forward. These functions are not included here for brevity, but refer to [3] for details on this derivation for the iso-morphic problem in the global ocean.

The POD ROM is then derived by first substituting decompositions of the prognostic variables into (8) and (9). The decompositions are given by substituting the forms of the trend, seasonal and anomalous components into (1) giving

$$\boldsymbol{u}(\boldsymbol{x},t) = \bar{\boldsymbol{u}}^{PI}(\boldsymbol{x}) + [T^G(t) - T^G(t^{PI})]\frac{\Delta\bar{\boldsymbol{u}}}{\Delta T^G}(\boldsymbol{x}) + \sum_{\vartheta=Jan}^{Dec}\tilde{\boldsymbol{u}}^{\vartheta}(\boldsymbol{x})\,d^{\vartheta}(t) + \sum_{n=1}^{Nu}\boldsymbol{\mathcal{U}}^{(n)}(\boldsymbol{x})\,a^{(n)}(t)\,, \text{ and} \quad (6)$$

$$T(\boldsymbol{x},t) = \bar{T}^{PI}(\boldsymbol{x}) + [T^G(t) - T^G(t^{PI})]\frac{\Delta T}{\Delta T^G}(\boldsymbol{x}) + \sum_{\vartheta=Jan}^{Dec}\tilde{T}^{\vartheta}(\boldsymbol{x})\,d^{\vartheta}(t) + \sum_{n=1}^{N_T}\mathcal{T}^{(n)}(\boldsymbol{x})\,b^{(n)}(t)\,. \quad (7)$$

One then projects the equations of motion onto the appropriate POD modes. The evolution of the velocity field is derived by symbolically applying the velocity inner product between the momentum equation in (8) and the n-th velocity spatial mode, $\boldsymbol{\mathcal{U}}^{(n)}(\boldsymbol{x})$. Expanding the terms and applying orthogonality properties, results in the ODEs

$$\dot{a}^{(n)}(t) = \sum_{\vartheta=Jan}^{Dec}[D_n^{\vartheta}\dot{d}^{\vartheta}(t) + B_n^{\vartheta}T^G(t)d^{\vartheta}(t) + C_n^{\vartheta}d^{\vartheta}(t) + \sum_{\vartheta'=Jan}^{Dec}F_n^{\vartheta\vartheta'}d^{\vartheta}(t)d^{\vartheta'}(t) + \sum_{m=1}^{Nu}L_{nm}^{\vartheta}a^{(m)}(t)d^{\vartheta}(t)]$$
$$+ A_n\dot{T}^G(t) + H_n[T^G(t)]^2 + \sum_{m=1}^{Nu}\sum_{k=1}^{Nu}Q_{nmk}a^{(m)}(t)a^{(k)}(t) + \sum_{m=1}^{N_T}Z_{nm}b^{(m)}(t) + \sum_{m=1}^{Nu}Y_{nm}a^{(m)}(t)T^G(t) \quad (10)$$

where the dot superscript denotes the time derivative. We produce the ODEs for the temperature field using an analogous approach. We apply the temperature inner product between the energy equation in (9) and the n-th temperature spatial mode, $\mathcal{T}^{(n)}(\boldsymbol{x})$, then apply the orthogonality properties to give

$$\dot{b}^{(n)}(t) = \sum_{\vartheta=Jan}^{Dec}[\check{D}_n^{\vartheta}\dot{d}^{\vartheta}(t) + \check{B}_n^{\vartheta}T^G(t)d^{\vartheta}(t) + \check{C}_n^{\vartheta}d^{\vartheta}(t) + \sum_{\vartheta'=Jan}^{Dec}\check{F}_n^{\vartheta\vartheta'}d^{\vartheta}(t)d^{\vartheta'}(t) + \sum_{m=1}^{N_T}\check{L}_{nm}^{\vartheta}b^{(m)}(t)d^{\vartheta}(t)]$$
$$+ \sum_{\vartheta=Jan}^{Dec}\sum_{m=1}^{N_T}\check{Z}_{nm}^{\vartheta}a^{(m)}(t)d^{\vartheta}(t) + \sum_{m=1}^{Nu}\check{W}_{nm}a^{(m)}(t)T^G(t)$$
$$+ \check{A}_n\dot{T}^G(t) + \check{H}_n[T^G(t)]^2 + \sum_{m=1}^{Nu}\sum_{k=1}^{Nu}\check{Q}_{nmk}b^{(m)}(t)a^{(k)}(t) + \sum_{m=1}^{N_T}\check{Y}_{nm}b^{(m)}(t)T^G(t) \quad (11)$$

All the terms without explicit time dependencies in the above ODEs are time invariant coefficients. All these coefficients also have analytical expressions, and can in principle be calculated from the known spatial modes, phase averages, and climate change gradient fields. However, here we instead use the structure of the ODEs to identify the appropriate input and output factors to solve regression problem, $\boldsymbol{Y} = \boldsymbol{\beta X} + \boldsymbol{\epsilon}$, where $\boldsymbol{\beta}$ is a vector containing the POD ROM coefficients, and the residuals. As per the left-hand-side of the ODEs, is a vector containing the time derivatives of the POD temporal modes. The input factors contained in the matrix are the groups of time varying terms on the right-hand-side. We solve for $\boldsymbol{\beta}$ using ridge regression, penalising for the squared distance to the data, and the square of the model coefficients.

Temporal Integration

In the POD ROM to follow we retained the first 10 velocity and temperature modes. We then determine the coefficients using samples taken from all 96 members of the CAFE-60 ensemble from 1970 to 2020. The temporal modes are also temporally interpolated, decreasing the time step size by a factor of 30, for numerical stability of the POD ROM. This results in a total of 1.728 million available samples. A fourth order Runge-Kutta scheme marches forward the coupled ODEs in (10) and (11), using the calculated POD ROM coefficients, with the globally averaged surface temperature prescribed. The ODEs are additionally perturbed with stochastic forcing representative of . The initial conditions of the POD ROM take on the values of the temporal velocity POD modes at the first time instant.

Figure 3(a) compares the first velocity temporal POD mode (black line) to the evolution of this mode as simulated by the POD ROM (red line). The variability is well represented, as are the magnitudes of the extreme values and dominant frequencies. The same is true for the first temperature mode in figure 3(d). As expected, the time series are out of phase. This is an illustration of the butterfly effect, due to the error growth in nonlinear dynamical systems.

*Corresponding Author, V. Kitsios vassili.kitsios@csiro.au

The only way to ensure specific events align is to run the POD ROM within a data assimilation system. A fairer relevant comparison is based on the statistics. Figure 3(b) and 3(c), illustrates that the variance and one-month autocorrelations of the velocity modes in the dynamically simulated POD ROM matches those in the underlying data. There are some differences, but the POD ROM broadly captures the variability and two-time statistics of the system within the resolved modes. The same can also be said for the variability and autocorrelations of the temperature modes respectively illustrated in figure 3(e) and 3(f).

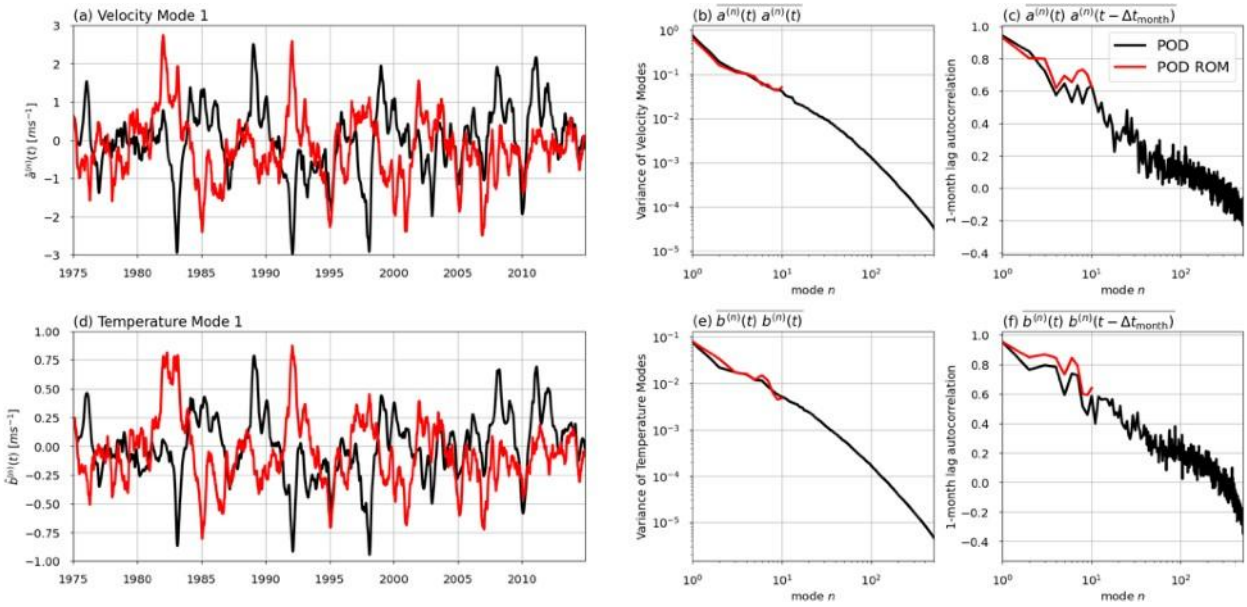

Figure 3 *Validation of POD ROM output with underlying temporal POD modes. Comparison of velocity temporal POD modes based on the: (a) time series; (b) POD energy spectra; and (c) one-month autocorrelation. Comparison of temperature temporal POD modes based on the: (d) time series; (e) POD energy spectra; and (f) one-month autocorrelation.*

Concluding Remarks

A reduced-order dynamical system was developed for the global atmosphere over the period from 1970 to 2020, as represented within the CAFE-60 reanalysis. The seasonal, anomalous climate variability and climate change trend components were explicitly decomposed. The trend response and seasonal cycles of the prognostic variables were calculated and sampled from the underlying data. The evolution of the anomalous component was governed by a POD ROM, derived by projecting the atmospheric equations of motion onto velocity and temperature POD mode bases. The coefficients in the POD ROM were calculated via a ridge regression approach, where the input and output factors were justified by the equations of motion. The POD ROM reproduced the statistics of the large-scale structures at a fraction of the computational cost required to numerical simulate such a flow.

References

1. Kitsios, V., O'Kane, T.J. & Newth, D. 2023 A machine learning approach to rapidly project climate responses under a multitude of net-zero emission pathways. Nature Communications Earth and Environment 4 (355), 1–15.

2. Perret, L., Collin, E. & Delville, J. 2006 Polynomial identification of pod based low-order dynamical system. Journal of turblence 7 (17).

3. Kitsios, V., Cordier, L & O'Kane, T.J. 2024 Proper orthogonal decomposition reduced-order model of the global oceans. Theor. Comput. Fluid Dyn. doi.org/10.1007/s00162-024-00719-9

4. Kitsios, V., Cordier, L. & O'Kane, T., Proper orthogonal decomposition reduced-order model of an hydrostatic atmosphere, 24th Australasian Fluid Mechanics Conference, Canberra, Australia, 1-5 December, 2024. doi.org/10.5281/zenodo.14213353

5. O'Kane, T.J., Sandery, P.A., Kitsios, V., Sakov, P., Matear, R.J., Chamberlain, M.A., Collier, M.A., Fiedler, R., Chapman, C., Moore, T.S. & Sloyan, B., 2021, CAFE60v1: A 60-year large ensemble climate reanalysis. Part I: System design, model configuration and data assimilation, Journal of Climate, 34 (13), 5153-5169. doi.org/10.1175/JCLI-D-20-0974.1

*Corresponding Author, V. Kitsios vassili.kitsios@csiro.au

6. Mitchell, T. D. 2003 Pattern scaling: An examination of the accuracy of the technique for describing future climates. Climatic Change 60, 217–242.

7. Cordier, L. & Bergmann, M. 2008 Proper Orthogonal Decomposition: an overview. In Lecture series 2008 on post-processing of experimental and numerical data. Von Karman Institute for Fluid Dynamics.

*Corresponding Author, V. Kitsios vassili.kitsios@csiro.au